Effect of pressure and temperature on energy transfer between Cr^{3+} and Tm^{3+} in $Y_3Al_5O_{12}$

Yongrong Shen, Toni Riedener, and Kevin L. Bray
Department of Chemistry and Institute for Shock Physics, Washington State University, Pullman, Washington 99164
(Received 12 August 1999)

We present variable temperature (15–295 K) and pressure (ambient–102 kbar) studies of energy transfer in Cr^{3+}:Tm^{3+}:YAG. The $Cr^{3+}\rightarrow Tm^{3+}$ energy-transfer rate was observed to increase with increasing temperature and to decrease with increasing pressure. The temperature study permitted us to identify three principal contributions to the overall energy-transfer rate from Cr^{3+}: thermally activated transfer from the $^4T_2$ state, thermally activated transfer from the anti-Stokes sidebands of the ^2E state, and temperature independent transfer from the zero phonon and Stokes sideband transitions of the ^2E state. High pressure permitted us to increase the energy of the $^4T_2$ state relative to the ^2E state and to eliminate the contribution of the $^4T_2$ state to the energy-transfer process. As a result, the contribution of the ^2E state to the energy-transfer process was isolated and evaluated independently. A quantitative model based on Förster-Dexter theory was used to determine the energy-transfer rates as a function of temperature and pressure. Comparisons of limiting high-pressure and low-temperature energy-transfer rates with the energy-transfer rate at ambient conditions allowed us to separate and determine the relative importance of the three principal energy-transfer processes at ambient conditions. We found that energy transfer from the $^4T_2$ state is dominant at ambient conditions despite the fact that it is $\sim$800 cm^{-1} higher in energy than the ^2E state. Deviations from the Inokuti-Hirayama energy-transfer model observed under low-temperature or high-pressure conditions were shown to be due to preferential energy transfer to nonrandomly distributed Tm^{3+} acceptors. At high-temperature or low-pressure conditions, the overall energy-transfer rate is sufficiently fast to permit efficient transfer to the more numerous randomly distributed Tm^{3+} acceptors. Under these conditions, the Inokuti-Hirayama model becomes a valid description.

I. INTRODUCTION

Energy-transfer processes remain an active area of investigation because of the central role they play in the design of new laser and phosphor materials. The fundamental energy-transfer process involves excitation of a donor species followed by transfer of the excitation energy in whole or in part to an acceptor species through a radiative or nonradiative mechanism. The acceptor species becomes excited and subsequently emits. Potential donor and acceptor species include lattice band states, molecular inorganic or organic units, and metal ions. Molecular units and metal ions can be present in the lattice composition or incorporated as dopants. In addition to simple transfer from one donor species to one acceptor species, transfer schemes involving multiple donor and/or acceptor species are possible. As a result, tremendous latitude in developing materials that operate over a wide range of excitation and emission wavelengths is available. Recent progress on energy transfer in the ultraviolet and down conversion further extends the range of possibilities.[1]

Energy transfer can occur through exchange, multipolar, and radiative mechanisms.[2,3] Of the systems studied to date, multipolar energy transfer based on the Förster-Dexter model is the most common mechanism.[4,5] According to the Förster-Dexter model, the rate of energy transfer from the donor species D to the acceptor species A is given by

$$W_{DA}=\frac{2\pi}{\hbar}|\langle D_g A_e|H_{DA}|D_e A_g\rangle|^2\int g_D(E)g_A(E)dE, \quad (1)$$

where the subscripts g and e refer to the ground and excited electronic states of the donor and acceptor species and H_{DA} is the multipolar D-A interaction Hamiltonian. The integral represents the spectral overlap between the normalized donor emission ($D_e\rightarrow D_g$) and normalized acceptor absorption ($A_g\rightarrow A_e$) line-shape functions $g_D(E)$ and $g_A(E)$, respectively.

In order to fully exploit the potential of energy transfer in designing materials that operate efficiently at new wavelengths, we need to understand the underlying physical processes responsible for energy transfer. In the case of Förster-Dexter energy transfer [Eq. (1)], optimization of the energy-transfer rate requires an understanding of the properties of the donor and acceptor electronic states. The strength of the donor-acceptor interaction and extent of spectral overlap are the key factors in determining the rate of energy transfer. These factors depend not only on the intrinsic electronic properties of the donor and acceptor, but also on the interaction of donors and acceptors with the surrounding lattice. The local coordination environments of donors and acceptors, along with their spatial proximity and strength of coupling to the lattice, ultimately determine the properties of electronic states necessary for energy transfer and the efficiency of energy transfer relative to internal radiative and nonradiative decay processes of the donor species.

Transition-metal (TM) ions are desirable donor species for many laser applications because they possess broad absorption bands that efficiently couple to conventional flashlamp pumping sources. TM ions are also photochemically stable and suitable for high power applications. Cr^{3+}, in particular, has been widely used as a donor in combination with rare-earth (RE) ion acceptors. The broad $^4T_2\rightarrow{}^4A_2$ emission of Cr^{3+} occurring in the red–near infrared strongly overlaps absorption transitions of many RE ions. Once excited, RE ions subsequently emit further into the near infra-

red. The growing need for efficient lasers at new wavelengths in the near infrared further motivates research on the energy-transfer properties of Cr^{3+}. The demonstration of improved near-infrared lasing efficiency of Nd^{3+} and Er^{3+} in garnets[6,7] has prompted several recent studies of energy transfer from Cr^{3+} to RE ions in a range of host materials.[8–24]

From the point of view of electronic structure, Cr^{3+} is an interesting donor species because in many host materials, its first excited state consists of strongly mixed ^2E and $^4T_2$ states. The two states interact electronically through the spin-orbit interaction and are sufficiently close in energy to have populations that vary significantly with temperature. As a result, the energy-transfer properties of Cr^{3+} are influenced by two electronic states that have different electronic configurations [$t_2^3(^2E)$ and $t_2^2e(^4T_2)$] and vastly different luminescence properties to the $^4A_2(t_2^3)$ ground state. By controlling temperature, we can systematically vary the relative populations of the ^2E and $^4T_2$ states and dramatically alter the luminescence and energy-transfer properties of Cr^{3+} in many systems. In the garnet systems $Gd_3Ga_5O_{12}$ and $Y_3Ga_5O_{12}$, for example, the luminescence of Cr^{3+} can be transformed from sharp line $^2E \rightarrow {}^4A_2$ emission at 10 K to broadband $^4T_2 \rightarrow {}^4A_2$ emission at room temperature.[25,26] Similarly, the energy-transfer rate and efficiency from Cr^{3+} to Tm^{3+} (Ref. 8) and Nd^{3+} (Ref. 19) in the strong field $Y_3Al_5O_{12}$ (YAG) lattice have been shown to be strong functions of temperature due to the thermal variation of the $^4T_2$ population.

In addition to temperature, high pressure can also significantly influence the luminescence properties of Cr^{3+} by varying the relative influence of the ^2E and $^4T_2$ states. With pressure, we alter the thermal populations of the ^2E and $^4T_2$ states by changing the energy separation between the two states. Because of its strong dependence on crystal-field strength, the energy of the $^4T_2$ state increases significantly with pressure.[27–32] The energy of the ^2E state, on the contrary, depends only weakly on crystal-field strength and is instead controlled by covalency effects. As a result, the energy of the ^2E state decreases weakly with pressure.[27–34] The net effect of pressure on Cr^{3+} therefore is to increase the energy difference between the $^4T_2$ and ^2E states. By varying this energy difference with pressure, we affect not only the thermal populations of the two states, but also the strength of their spin-orbit coupling. As the energy of the $^4T_2$ state increases relative to that of the ^2E state, the extent of spin-orbit coupling decreases and the influence of the $^4T_2$ state on the luminescence of Cr^{3+} is further weakened beyond the effect of thermal population.

We recently presented a preliminary high-pressure study of energy transfer in Cr^{3+}:Tm^{3+}:YAG.[17] Our objective was to use pressure to systematically vary the energy difference between the ^2E and $^4T_2$ states in an attempt to investigate the role of the $^4T_2$ state on the energy transfer of Cr^{3+}. We concluded that energy transfer from Cr^{3+} occurred more slowly, but more efficiently with increasing pressure as the contribution from the $^4T_2$ state was progressively diminished. Quantitative attempts to model the energy transfer using the Inokuti-Hirayama version[35] of Förster-Dexter dipole-dipole energy transfer, however, became increasingly inadequate with increasing pressure as the energy of the $^4T_2$ state increased. A similar behavior was observed in a temperature dependent study at low temperature as the thermal population of the $^4T_2$ state was decreased.[8]

In this paper, we consider dipole-dipole energy transfer in Cr^{3+}:Tm^{3+}:YAG in the context of Förster-Dexter theory without assuming a random distribution of acceptors as in the Inokuti-Hirayama treatment. We consider an additive model based on a pairwise $Cr^{3+} \rightarrow Tm^{3+}$ energy transfer to Tm^{3+} acceptors located in several neighboring coordination shells relative to the Cr^{3+} donor. The donor-acceptor distance for each acceptor coordination shell was obtained from known crystallographic data for YAG. By applying the model to temperature and pressure dependent energy-transfer rate data, we were able to identify regimes of validity of the Inokuti-Hirayama treatment. We were also able to determine that the breakdown of the Inokuti-Hirayama model at low-temperature and high-pressure conditions was due to preferential energy transfer among closely associated $Cr^{3+} \rightarrow Tm^{3+}$ pairs.

We also show that three primary energy-transfer pathways from Cr^{3+} are present: thermally activated energy transfer from the $^4T_2$ state, thermally activated energy transfer from the ^2E anti-Stokes phonon sidebands, and the temperature-independent energy transfer from the zero phonon and Stokes intensity of the ^2E state. We further show that the $^4T_2$ contribution to energy transfer is sensitive to pressure and can be eliminated above ~60 kbar at low temperature. By controlling temperature and pressure, we are able to resolve and independently evaluate the three transfer pathways.

II. EXPERIMENTAL DETAILS

High-pressure luminescence and decay experiments were performed using a modified Merrill-Bassett diamond-anvil cell (DAC). The samples were contained within a hole (200–250 μm in diameter) in an Inconel gasket between two diamonds. A 4:1 methanol:ethanol mixture and ruby were used as a pressure transmitting medium and as a pressure calibrant, respectively. For low-temperature experiments, the samples were cooled by a closed-cycle helium refrigerator which provided a temperature range from 12 K to room temperature.

The pulsed excitation at 580 nm was provided by a pulsed dye laser (Spectra Physics PDL3, Rhodamine 590 dye) pumped by the second harmonic of a Nd^{3+}:YAG laser (Continuum NY61-10). The luminescence was dispersed by a 1-m monochromator (Spex-1704 with 1200 grooves/mm grating blazed at 500 nm) and detected by a photomultiplier tube (Hamamatsu R928) using a standard photon counting technique. The luminescence decay data were collected by a digital storage oscilloscope (Lecroy-LS140 100 MHz) capable of averaging over 1000 signal pulses. Continuous-wave (CW) luminescence was excited with the 465.8- and 488-nm lines of an Ar^+ laser (Lexel 95L) or the 580 nm line from a CW dye laser (Spectra Physics 375B, 580 – 620 nm output from a Rhodamine 590 dye) pumped by the Ar^+ laser. All luminescence spectra were corrected for instrumental response.

The Cr^{3+}(0.5 at.%):YAG, Tm^{3+}(2 at.%):YAG, and

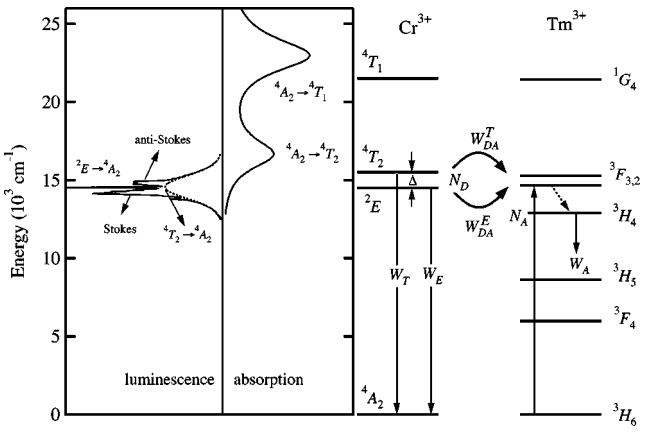

FIG. 1. Schematic energy-level diagrams of Cr^{3+} and Tm^{3+} in YAG showing the energy transfer from Cr^{3+} to Tm^{3+}. The absorption and luminescence spectra of Cr^{3+}(0.5 at. %):YAG are shown at ambient pressure and room temperature.

Cr^{3+}(0.7 at. %):Tm3+(2 at. %):YAG samples used in the present study were obtained from Scientific Materials Corporation (Bozeman, MT).

III. RESULTS AND DISCUSSION

A. Theoretical background

Figure 1 shows a schematic energy level diagram of Cr^{3+} and Tm^{3+} ions in YAG. The absorption and emission spectra at ambient pressure are also shown. The energy difference $\Delta = E(^4T_2) - E(^2E)$ is approximately 800 cm^{-1} in Cr^{3+}:YAG at ambient conditions and is sufficiently small to permit a small thermal population of the $^4T_2$ state. As a result, the luminescence consists of two $^2E \rightarrow {}^4A_2$ zero phonon lines (R lines) and accompanying Stokes and anti-Stokes phonon sidebands superimposed on a broad underlying $^4T_2 \rightarrow {}^4A_2$ band. With decreasing temperature,[36–38] the $^4T_2 \rightarrow {}^4A_2$ band and the anti-Stokes phonon sidebands are gradually diminished due to the thermal depopulation.

For Tm^{3+} in YAG, three groups of absorption lines appear in the visible and correspond to transitions from the $^3H_6$ ground state to the $^3H_4$ (~780 nm), $^3F_{2,3}$ (~680 nm), and $^1G_4$ (~460 nm) excited states.[39–42] Upon excitation to the $^1G_4$ state (λ_{ex}=465.8 nm), Tm^{3+}:YAG luminescence has been observed between 770 and 850 nm and has been attributed to $^1G_4 \rightarrow {}^3H_5$ (Ref. 42) and $^3H_4 \rightarrow {}^3H_6$ emission [Fig. 2(a)]. Figure 2(b) shows Tm^{3+} emission in Cr^{3+}:Tm^{3+}:YAG upon simultaneous excitation of Cr^{3+} ($^4A_2 \rightarrow {}^4T_1$) and Tm^{3+} ($^3H_6 \rightarrow {}^1G_4$) ($\lambda_{ex}$ =465.8 nm). Codoping with Cr^{3+} introduces an energy-transfer pathway for exciting Tm^{3+} into its $^3F_{2,3}$ states and leads to an enhancement of the $^3H_4 \rightarrow {}^3H_6$ emission of Tm^{3+} relative to the $^1G_4 \rightarrow {}^3H_5$ emission. When an excitation wavelength (λ_{ex}=488.0 nm) capable of exciting the Cr^{3+} $^4T_1$ state, but not the Tm^{3+} $^1G_4$ level, was used to excite Cr^{3+}:Tm^{3+}:YAG, the strong Tm^{3+} $^3H_4 \rightarrow {}^3H_6$ luminescence remained while the Tm^{3+} $^1G_4 \rightarrow {}^3H_5$ luminescence completely disappeared [Fig. 2(c)]. These observations indicate that $Cr^{3+} \rightarrow Tm^{3+}$ energy transfer occurs from the

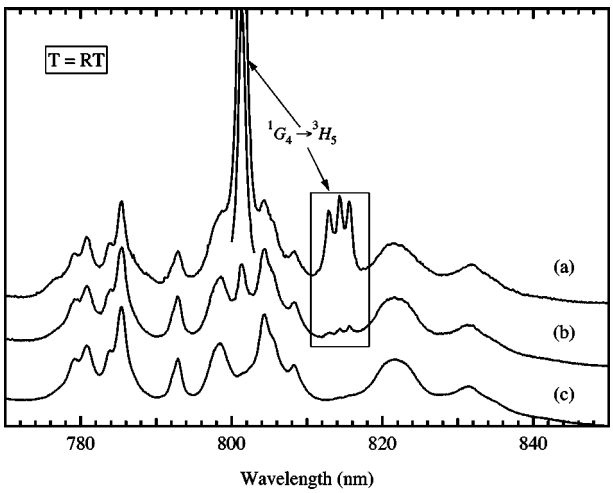

FIG. 2. Ambient pressure and room temperature $^1G_4 \rightarrow {}^3H_5$ and $^3H_4 \rightarrow {}^3H_6$ luminescence in (a) Tm^{3+}(2 at. %):YAG upon excitation of the $^1G_4$ state (λ_{ex}=465.8 nm), (b) Cr^{3+}(0.7 at. %):Tm^{3+} (2 at. %):YAG upon simultaneous excitation of the Tm^{3+} ($^3H_4 \rightarrow {}^1G_4$) and Cr^{3+} ($^4A_2 \rightarrow {}^4T_1$) ($\lambda_{ex}$=465.8 nm), and (c) Cr^{3+}(0.7 at. %):Tm^{3+}(2 at. %):YAG upon excitation of only the Cr^{3+}($^4A_2 \rightarrow {}^4T_1$) ($\lambda_{ex}$=488.0 nm).

$^4T_2$ and ^2E states of Cr^{3+} to the $^3F_{2,3}$ states of Tm^{3+}, but not directly from the $^4T_1$ state of Cr^{3+} to the $^1G_4$ state of Tm^{3+}.

The luminescence spectrum of Cr^{3+}:Tm^{3+}:YAG at ambient conditions (Fig. 3) indicates that radiative energy transfer from the $^4T_2$ and ^2E states of Cr^{3+} to the $^3F_{2,3}$ levels of Tm^{3+} also occurs as evidenced by the missing intensity in the anti-Stokes region of the spectrum relative to Cr^{3+}:YAG (Fig. 1).

The $Cr^{3+} \rightarrow Tm^{3+}$ energy-transfer pathway is illustrated in Fig. 1. The dynamic rate equations describing the time dependence of the energy-transfer process are given by

$$\frac{dN_D}{dt} = -W_D N_D - \frac{dP_{DA}(t)}{dt} N_D ,$$

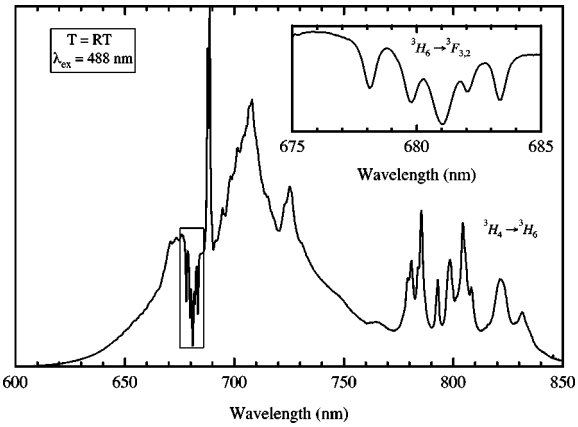

FIG. 3. Ambient pressure and room-temperature luminescence spectrum of Cr^{3+}(0.7 at. %):Tm^{3+}(2 at. %):YAG upon Cr^{3+} ($^4A_2 \rightarrow {}^4T_1$) excitation at λ_{ex}=488.0 nm. Coupled $^4T_2$, $^2E \rightarrow {}^4A_2$ emission from Cr^{3+} and the $^3H_4 \rightarrow {}^3H_6$ emission of Tm^{3+} resulting from energy transfer were observed. The inset shows the Tm^{3+} ($^3H_6 \rightarrow {}^3F_{2,3}$) absorption spectrum.

$$\frac{dN_A}{dt} = -W_A N_A + \frac{dP_{DA}(t)}{dt} N_D, \tag{2}$$

where N_D is the number of Cr^{3+} donor ions in the thermally coupled $^4T_2$-^2E excited states and N_A is the number of Tm^{3+} acceptor ions excited into the $^3F_{2,3}$ levels by energy transfer. Since rapid multiphonon relaxation occurs from the $^3F_{2,3}$ levels to the $^3H_4$ emitting level of Tm^{3+}, $Tm^{3+} \rightarrow Cr^{3+}$ back transfer can be neglected and N_A also represents the number of Tm^{3+} ions in the $^3H_4$ level. W_D and W_A are the internal (intracenter) decay rates for the coupled $^4T_2$-^2E states of Cr^{3+} and the $^3H_4$ level of Tm^{3+}, respectively, and $P_{DA}(t)$ is the $D \rightarrow A$ energy-transfer function. In addition to radiative and nonradiative decay from the $^3H_4$ state, the internal decay rate W_A of Tm^{3+} includes the rate of the cross-relaxation process $(^3H_4, {}^3H_6) \rightarrow (^3F_4, {}^3F_4)$ known to occur in YAG at Tm^{3+} concentrations above $\sim 0.75\%$.[43] In the remainder of the paper, we make no attempt to resolve cross-relaxation effects from other processes occurring from the $^3H_4$ state of Tm^{3+}.

Solving Eq. (2) for the donor decay gives

$$N_D(t) = N_D(0) \exp(-W_D t) \exp[-P_{DA}(t)], \tag{3}$$

where $N_D(0)$ is the number of donors excited at $t=0$. When no *D-D* transfer occurs, the energy-transfer function $P_{DA}(t)$ can be written in a general form:[3,44,45]

$$P_{DA}(t) = \sum_l \ln\{1 - C_A + C_A \exp[-W_{DA}(l)t]\},$$

where C_A is the probability that an acceptor site is occupied by an acceptor (equivalent to the acceptor atom fraction doping concentration) and l indexes all potential acceptor sites in the lattice. $W_{DA}(l)$ is the energy-transfer rate from a donor ion to an acceptor ion in site l. Instead of indexing individual acceptors, we can rewrite $P_{DA}(t)$ in terms of sets of equivalent acceptor ions located at a common distance from the donor ion to obtain

$$P_{DA}(t) = \sum_s N_s \ln\{1 - C_A + C_A \exp[-W_{DA}(R_s)t]\}, \tag{4}$$

where the sum is now over all coordination shells s each containing N_s equivalent acceptor sites located at a distance R_s from the donor. In obtaining Eq. (4), we are implicitly assuming that the transfer rate $W_{DA}(R_s)$ is the same for transfer to all acceptor ions in coordination shell s. Since multisite behavior has been reported for Tm^{3+} in YAG,[20] the values of $W_{DA}(R_s)$ obtained in our analysis are intended to represent averages over all sites at distances R_s from a donor. Resolution of the small site-to-site differences in local configuration and energy-level structure are beyond the model presented in this work. In Cr^{3+}:Tm^{3+}:YAG, Tm^{3+} occupies dodecahedral Y^{3+} (c) sites and Cr^{3+} occupies octahedral Al^{3+} (a) sites. The number of sites contained in and the radii of the first ten acceptor Y^{3+} (c) coordination shells relative to a donor ion located at the origin of a reference coordinate system in the YAG lattice are given in Table I. Based on a multipolar interaction, the energy-transfer rate from a Cr^{3+} donor to an acceptor in the sth shell is described by $W_{DA}(R_s) = \alpha_{DA}^{(m)}/R_s^m$ where $m=6$ (dipole-dipole), 8 (dipole-quadrupole), or 10 (quadrupole-quadrupole) denotes the multipolar interaction mechanism. $\alpha_{DA}^{(m)}$ is the *D-A* energy-transfer constant and is proportional to the spectral overlap of donor emission and acceptor absorption. In the context of our model, which averages over multisites, $\alpha_{DA}^{(m)}$ is a constant for all donor and acceptor pairs in the lattice. As a result, the relative energy-transfer rates from a donor to acceptors in different coordination shells are given by $W_{DA}(R_s)/W_{DA}(R_{s+1}) = (R_{s+1}/R_s)^m$. Values of each multipolar mechanism are included in Table I.

TABLE I. Relative energy-transfer rates from a reference Cr^{3+} donor to Tm^{3+} acceptors in different Y^{3+} coordination shells in YAG at ambient pressure. The reference Cr^{3+} donor is assumed to be located at the origin of the coordinate system. s indexes Y^{3+} coordination shells. N_s is the number of Y^{3+} sites in the sth coordination shell and R_s is the distance of Y^{3+} sites in shell s from the reference Cr^{3+} donor. Energy-transfer rates to Tm^{3+} ions in shell s relative to shell $s+1$ are shown for various multipolar energy-transfer mechanism ($m=6$, 8, and 10). The distances R_s are obtained from the known crystal structure and lattice constant (12 Å) of YAG. (Ref. 48).

			$W_{DA}(R_s)/W_{DA}(R_{s+1})$		
s	N_s	R_s(Å)	$m=6$	$m=8$	$m=10$
1	6	3.354	17.573	45.687	118.778
2	6	5.408	4.217	6.814	11.009
3	12	6.874	2.634	3.637	5.023
4	18	8.078	2.076	2.649	3.379
5	6	9.124	1.799	2.188	2.661
6	18	10.062	1.634	1.924	2.267
7	18	10.920	1.524	1.755	2.019
8	18	11.715	1.448	1.638	1.852
9	24	12.460	1.389	1.550	1.730
10	24	13.162	1.345	1.485	1.639

The temporal evolution of the number of acceptor ions excited through energy transfer is obtained by solving the rate equations given in Eq. (2). By substituting $N_D(t)$ in Eq. (2) with Eq. (3) and using the initial conditions $N_D(t=0) = N_D(0)$ and $N_A(t=0) = 0$, we obtain the time dependence $N_A(t)$ of the excited acceptor ion population

$$N_A(t) = N_D(0)\{\exp[-W_D t - P_{DA}(t)] - \exp(-W_A t) + \phi(t)\}, \tag{5}$$

where

$$\phi(t) = (W_A - W_D)\exp(-W_A t) \times \int_0^t \exp[(W_A - W_D)\tau - P_{DA}(\tau)]\, d\tau. \tag{6}$$

Generally, the integral in Eq. (6) cannot be solved analytically due to the complex form of the transfer function $P_{DA}(t)$. Rigorous evaluation of the excited acceptor population is therefore difficult. We can, however, estimate the time evolution by approximating $P_{DA}(t)$ as a linear function of time, given by $P_{DA}(t) = \overline{W}_{DA} t$,[20] where $\overline{W}_{DA}$ is defined as an average or effective-transfer rate. Under this approximation, Eq. (6) becomes

$$\phi(t)=\frac{W_A-W_D}{W_A-(W_D+\overline{W}_{DA})}\exp[-(W_D+\overline{W}_{DA})t]. \quad (7)$$

Substitution of Eq. (7) into Eq. (5) leads to

$$N_A(t)=N_D(0)\left\{\left[1+\frac{W_A-W_D}{W_A-(W_D+\overline{W}_{DA})}\right]\times\exp[-(W_D+\overline{W}_{DA})t]-\exp(-W_At)\right\}. \quad (8)$$

Since the acceptor luminescence intensity is proportional to $N_A(t)$, Eq. (8) predicts that the acceptor luminescence intensity will exhibit an initial rise followed by a decay. From Eq. (8), we can expect that the acceptor luminescence will start from zero at $t=0$ and increase to a maximum at time $t_{\max}$ given by

$$t_{\max}=\frac{1}{(W_D+\overline{W}_{DA})-W_A}\ln\left\{\frac{(W_D+\overline{W}_{DA})}{W_A}\times\left[1+\frac{W_A-W_D}{W_A-(W_D+\overline{W}_{DA})}\right]\right\}. \quad (9)$$

For $t>t_{\max}$, the luminescence decays in time at a rate governed by the smaller of W_A and $W_D+\overline{W}_{DA}$.

Using Eqs. (8) and (9), we can estimate the influence of $D\rightarrow A$ energy transfer on the time evolution of the acceptor luminescence. Thus, for example, if $W_D=10^3\ s^{-1}$, $W_A=10^4\ s^{-1}$, and $\overline{W}_{DA}=10^7\ s^{-1}$ (fast energy transfer), the maximum acceptor luminescence intensity occurs at $t_{\max}\approx1.6\ \mu s$ and the rise ($t<t_{\max}$) is determined by the $D\rightarrow A$ energy-transfer rate, while the decay ($t>t_{\max}$) is determined by the acceptor decay (W_A). For a moderate energy-transfer rate, e.g., $\overline{W}_{DA}=10^5\ s^{-1}$, we obtain $t_{\max}\approx25.4\ \mu s$ and expect that the decay is still determined by W_A. If the energy transfer is very slow, e.g., $\overline{W}_{DA}=10^3\ s^{-1}$, we find $t_{\max}\approx121\ \mu s$ and that the acceptor decay is determined by the de-excitation of the donor system (W_D and $\overline{W}_{DA}$).

B. Temperature dependence

Ambient pressure luminescence decays for Cr^{3+} ions in Cr^{3+}:Tm^{3+}:YAG were obtained in the temperature range from 15 K to RT upon excitation to the $^4T_2$ state of Cr^{3+} ($\lambda_{ex}=580$ nm). The Cr^{3+} decay was nonexponential at all temperatures. Representative Cr^{3+} decay curves at 15 K, 150 K, and RT are shown in Fig. 4. The nonexponential decays directly reflect the presence of energy transfer from Cr^{3+} to Tm^{3+}. The Cr^{3+} luminescence intensity decreases sharply at short time due to rapid energy transfer to Tm^{3+} acceptors in close proximity. As time progresses, the nearby acceptors become saturated and energy transfer occurs to increasingly more distant acceptors. As the energy-transfer process becomes less competitive with internal Cr^{3+} decay, the rate of the Cr^{3+} intensity decrease slows and approaches the value found for Cr^{3+} in the absence of Tm^{3+} ions.

In order to obtain the $Cr^{3+}\rightarrow Tm^{3+}$ transfer rate from the Cr^{3+} decay data, Eqs. (3) and (4) were used to fit the

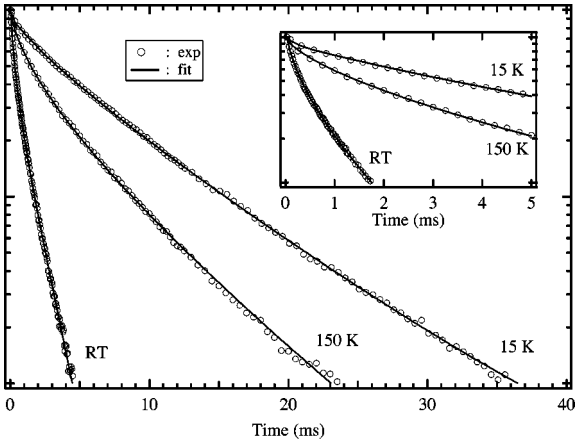

FIG. 4. Ambient pressure luminescence decays of Cr^{3+} in Cr^{3+}(0.7 at. %):Tm^{3+}(2 at. %):YAG at 15 K, 150 K, and RT upon excitation of Cr^{3+} ($^4A_2\rightarrow{}^4T_2$) ($\lambda_{ex}=580.0$ nm). Solid curves represent fits of the decay data using Eqs. (3) and (4) and assuming a dipole-dipole ($m=6$) energy-transfer mechanism.

temperature-dependent Cr^{3+} decay curves at ambient pressure. Since internal emission and energy transfer occur from the thermally coupled $^4T_2$ and ^2E states of Cr^{3+}, W_D, and W_{DA} are expressed according to a Boltzmann thermal equilibrium

$$W_D=\frac{W_E+W_T(g_T/g_E)\exp(-\Delta/k_BT)}{1+(g_T/g_E)\exp(-\Delta/k_BT)}, \quad (10)$$

and

$$W_{DA}=\frac{W_{DA}^E+W_{DA}^T(g_T/g_E)\exp(-\Delta/k_BT)}{1+(g_T/g_E)\exp(-\Delta/k_BT)}, \quad (11)$$

where $g_T=12$ and $g_E=4$ denote the degeneracies of the $^4T_2$ and ^2E states, Δ is the zero-phonon energy separation between the $^4T_2$ and ^2E states, W_T and W_E are the intrinsic decay rates of the $^4T_2\rightarrow{}^4A_2$ and $^2E\rightarrow{}^4A_2$ transitions of Cr^{3+}, and W_{DA}^T and W_{DA}^E are the energy transfer rates from the $^4T_2$ and ^2E states of Cr^{3+} to the $^3F_{2,3}$ levels of Tm^{3+}. A dipole-dipole ($m=6$) energy-transfer mechanism was assumed and $C_A=0.02$. Two parameters, W_D and W_{DA} [$=\Sigma_s W_{DA}(R_s)$], were treated as adjustable in the decay curve fits. Inclusion of the first eight shells in Table I resulted in excellent agreement between the experimental and calculated data over the whole temperature range. We note that temperature variations in the distances R_s in Table I do not need to be specifically considered because of the cubic symmetry of the unit cell of YAG. A consequence of the cubic symmetry is that all of the distances R_s scale identically with temperature induced changes in the lattice parameter. As a result, the ratios $W_{DA}(R_s)/W_{DA}(R_{s+1})$ given in Table I are independent of lattice parameter. Representative values of W_{DA} and W_D obtained from the fits are given in Table II. The corresponding decay curve fits are included as solid lines in Fig. 4.

The variation with temperature of the $Cr^{3+}\rightarrow Tm^{3+}$ transfer rate W_{DA} over the range of temperatures considered in this study is shown as open circles in Fig. 5. The temperature dependence of the Cr^{3+} lifetime ($\tau_D=W_D^{-1}$) obtained from

TABLE II. Ambient pressure values for the $Cr^{3+} \rightarrow Tm^{3+}$ transfer rate (W_{DA}) and the Cr^{3+} lifetime ($\tau_D = W_D^{-1}$) in Cr^{3+}(0.7 at. %):Tm^{3+}(2 at. %):YAG at 15 K, 150 K, and RT.

T	$W_{DA}(ms^{-1})$	τ_D (ms)
15 K	11	9.2
150 K	44	7.4
RT	404	1.6

the analysis was in excellent agreement with previously reported temperature studies of Cr^{3+}:YAG.[19,34,38] At temperatures below ~100 K, the transfer rate was nearly constant. As the temperature was increased above 100 K, the rate began to increase rapidly. The rapid increase in the transfer rate with increasing temperature is mainly due to the increased contribution of the $^4T_2$ state to the $Cr^{3+} \rightarrow Tm^{3+}$ energy-transfer process as its thermal population increases.

The temperature dependence of the transfer rate W_{DA} from the thermally coupled $^4T_2$ and ^2E states of Cr^{3+} can be described by Eq. (11). In analyzing the temperature dependence of the transfer rate, the temperature dependence of the energy separation Δ between the $^4T_2$ and ^2E states was taken into account. Δ was assumed to remain constant below 100 K and to decrease linearly with temperature above 100 K at a rate $d\Delta/dT = -0.1$ cm^{-1}/K derived from the reported shift rates of about -0.25 cm^{-1}/K for the $^4T_2$ state[46] and about -0.15 cm^{-1}/K for the ^2E state[34] above 100 K. A direct fit of Eq. (11) to the transfer rate data was completed and produced curve I of Fig. 5. The resulting optimized values for W_{DA}^E, W_{DA}^T, and Δ are presented in Table III. We see from Fig. 5 that Eq. (11) provides a satisfactory fit to the data for temperature below ~100 K. Above ~100 K, however, significant deviations from the data are found. Eq. (11) is unable to adequately describe thermally activated contributions to the energy-transfer process and the fitted value

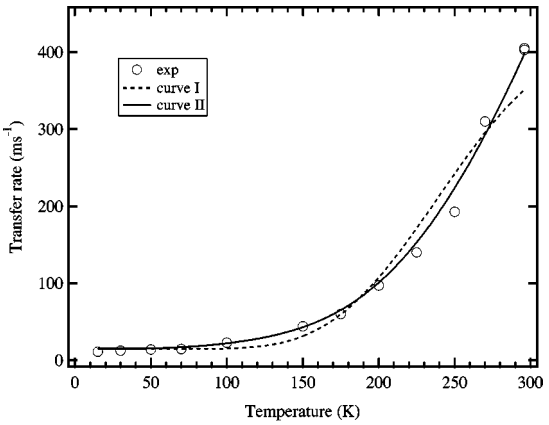

FIG. 5. Temperature dependence of the ambient-pressure $Cr^{3+} \rightarrow Tm^{3+}$ transfer rate W_{DA} in Cr^{3+}(0.7 at. %):Tm^{3+}(2 at. %):YAG. W_{DA} was obtained from fits of the experimental decay curves as a function of temperature using Eqs. (3) and (4) and assuming dipole-dipole energy transfer. Curve I represents the calculated result using Eq. (11) and the parameters given in Table III. Curve II represents the calculated result using Eq. (12) and the parameters given in Table III.

TABLE III. Parameters fitted to the experimental transfer rate data in Fig. 5. The value reported for Δ corresponds to the limiting low temperature value.

Curve	Eq.	W_{DA}^E (ms^{-1})	W_{DA}^T (ms^{-1})	$W_{DA}^{AS}(\infty)$ (ms^{-1})	Δ (cm^{-1})
I	(11)	15	6446		741
II	(12)	15	5783	499	842

$\Delta = 741$ cm^{-1} is lower than the value (828 cm^{-1}) reported for Cr^{3+} in YAG on the basis of recent temperature-dependent lifetime studies.[34]

We attribute the difference between the calculated and experimental energy-transfer rates to a neglect of the contribution of the temperature dependence of the Cr^{3+} anti-Stokes phonon sideband emission in Eq. (11). The anti-Stokes phonon sideband emission originates from the vibronic states of the ^2E state and exhibits a strong increase with temperature.[36–38] In Fig. 6, we explicitly show the increase in anti-Stokes luminescence intensity with increasing temperature in Cr^{3+}:Tm^{3+}:YAG. At 15 K, no anti-Stokes intensity was observed. Above ~75 K, anti-Stokes sidebands developed and rapidly gained intensity with increasing temperature. Since the anti-Stokes emission overlaps appreciably with the $^3F_{2,3}$ levels of Tm^{3+}, it provides an important temperature-dependent contribution to the energy-transfer rate that is not accounted for in the model of Eq. (11). The anti-Stokes contribution is expected to be a particularly important temperature-dependent process in the intermediate temperature region (~75–~175 K) because the thermal population of the $^4T_2$ state does not become appreciable until the temperature is ~175 K.

A more complete temperature analysis requires an extension of Eq. (11) to include the temperature dependence of the energy transfer from the ^2E vibronic states. Since thermal population of the ^2E vibronic states obeys the simple Boltzmann law, we assumed that the transfer rate from a ^2E vibronic state with phonon energy $\hbar\omega$ is proportional to $\overline{D}(\omega)\exp(-\hbar\omega/k_BT)$, where $\overline{D}(\omega)$ is the effective phonon density of states resulting from the electron-phonon interaction and is related to the low-temperature vibronic structure.

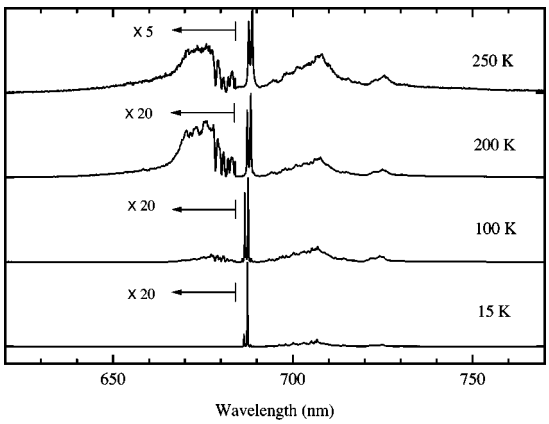

FIG. 6. Ambient pressure Cr^{3+} luminescence spectra of Cr^{3+}(0.7 at. %):Tm^{3+}(2 at. %):YAG at several temperatures upon CW excitation of Cr^{3+} ($^4A_2 \rightarrow {}^4T_2$) ($\lambda_{ex} = 580$ nm). The significant increase in anti-Stokes intensity with temperature is evident.

We have previously determined $\overline{D}(\omega)$ from the Stokes phonon sideband of the 15 K $^2E \rightarrow {}^4A_2$ luminescence spectrum of Cr^{3+}:YAG.[34] The total contribution of the ^2E vibronic states of Cr^{3+} to the $Cr^{3+} \rightarrow Tm^{3+}$ energy transfer can be derived by integrating over all phonon states according to

$$W_{DA}^{AS} = W_{DA}^{AS}(\infty) \int_0^\infty \overline{D}(\omega) \exp(-\hbar\omega/k_B T) d\omega,$$

where $W_{DA}^{AS}(\infty)$ is defined as the transfer rate from the ^2E vibronic states to Tm^{3+} in the limit of infinite temperature. $W_{DA}^{AS}(\infty)$ is expected to be much larger than the corresponding quantity W_{DA}^{E} for the ^2E zero-phonon state because the vibronic states are much closer in resonance to the $^3F_{2,3}$ levels of Tm^{3+} (Figs. 3 and 6). Thus the temperature dependence of the transfer rate can be described more fully by

$$W_{DA} = \frac{W_{DA}^{E} + W_{DA}^{AS}(\infty) \int_0^\infty \overline{D}(\omega) \exp(-\hbar\omega/k_B T) d\omega + W_{DA}^{T}(g_T/g_E) \exp(-\Delta/k_B T)}{1 + (g_T/g_E) \exp(-\Delta/k_B T)}. \quad (12)$$

A fit of Eq. (12) to the experimental data in Fig. 5 produced the optimized values of W_{DA}^{E}, W_{DA}^{T}, $W_{DA}^{AS}(\infty)$, and Δ given in Table III and curve II in Fig. 5. A substantial improvement in the quality of the fit is obtained when the temperature dependence of the transfer rate from the ^2E vibronic states is included. The energy separation (Δ) between the $^4T_2$ and ^2E states obtained in the present study is very close to the value reported for Cr^{3+}:YAG ($\Delta = 828\ cm^{-1}$) on the basis of recent temperature-dependent lifetime studies.[34]

C. Pressure dependence

Temperature affects the $Cr^{3+} \rightarrow Tm^{3+}$ energy-transfer process in Cr^{3+}:Tm^{3+}:YAG primarily through the thermal population of the $^4T_2$ state and the ^2E vibronic states. Pressure, on the contrary, directly induces a significant increase in Δ. As a result, pressure leads to a decrease in the thermal population of the $^4T_2$ state and a reduction in its contribution to the energy-transfer process. Since the energy of zero phonon and vibronic $^2E \rightarrow {}^4A_2$ transitions of Cr^{3+}:YAG change only weakly with pressure,[31,34] we expect little change in the energy-transfer properties of the ^2E state with pressure. The application of pressure therefore allow us to stablize a state in which energy transfer occurs exclusively from the ^2E state of Cr^{3+}.

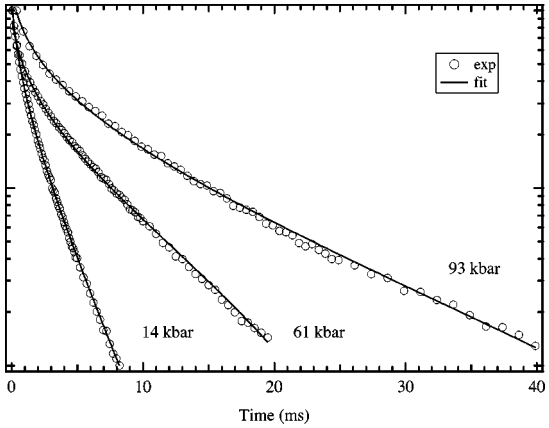

FIG. 7. Room-temperature luminescence decays of Cr^{3+} in Cr^{3+}(0.7 at. %):Tm^{3+}(2 at. %):YAG at 14, 61, and 93 kbar upon excitation of Cr^{3+}($^4A_2 \rightarrow {}^4T_2$) ($\lambda_{ex} = 580.0$ nm). The solid curves represent fits based on Eqs. (3) and (4) and assuming dipole-dipole energy transfer.

The RT Cr^{3+} luminescence decays of Cr^{3+}:Tm^{3+}:YAG were measured in three series of experiments over a pressure range of ~100 kbar (Fig. 7). The decay curves were analyzed using Eqs. (3) and (4) (assuming contributions from the first eight acceptor coordination shells and $m = 6$ as in the temperature study) to obtain the effect of pressure on the energy-transfer rate W_{DA}. As discussed in the temperature study, the cubic symmetry of the YAG lattice means that the $W_{DA}(R_s)/W_{DA}(R_{s+1})$ ratios given in Table I are independent of pressure. (Hua, Mirov, and Vohra[47] have shown that the cubic symmetry of YAG is preserved well beyond the upper pressure limit of this study.) Representative decay curve fits using the optimized values of W_{DA} and W_D shown in Table IV at 14, 61, and 93 kbar are shown in Fig. 7 and the variation of W_{DA} with pressure is shown in Fig. 8.

It is seen from Fig. 8 that the transfer rate exhibited a strong decrease at low pressure (<40 kbar) followed by a weaker decrease and leveling off at high pressure (>60 kbar). The strong decrease in transfer rate below ~40 kbar is due to the rapid elimination of energy transfer from the $^4T_2$ state as its thermal population is reduced. The leveling of the transfer rate above ~60 kbar corresponds to a regime in which energy transfer occurs almost exclusively from the ^2E zero phonon and vibronic states. The approximately constant energy transfer rate above ~60 kbar indicates that the ^2E energy-transfer properties do not vary significantly with pressure.

TABLE IV. Room-temperature values for the $Cr^{3+} \rightarrow Tm^{3+}$ transfer rate (W_{DA}) and the Cr^{3+} lifetime ($\tau_D = W_D^{-1}$) in Cr^{3+}(0.7 at. %):Tm^{3+}(2 at. %):YAG at 14, 61, and 93 kbar.

	Cr^{3+}(0.7 at. %):Tm^{3+}(2 at. %):YAG		Cr^{3+}(0.5 at. %):YAG (Ref. 34)
P (kbar)	W_{DA} (ms^{-1})	τ_D (ms)	τ_D (ms)
14	229	2.7	3.0
61	106	9.5	9.3
93	85	15	14.8

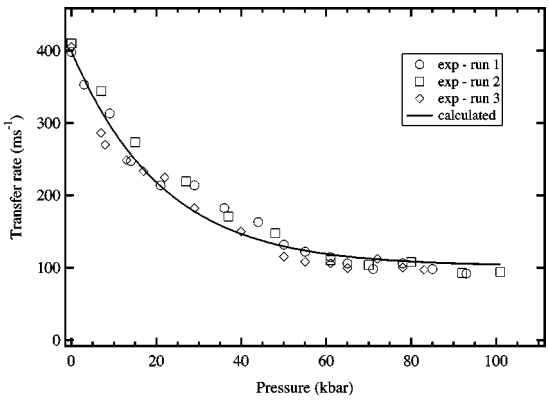

FIG. 8. Pressure dependence of the room-temperature $Cr^{3+} \rightarrow Tm^{3+}$ transfer rate W_{DA} in Cr^{3+}(0.7 at. %):Tm^{3+}(2 at. %):YAG. W_{DA} was obtained from fits of the experimental decay curves as a function of pressure using Eqs. (3) and (4) and assuming dipole-dipole energy transfer. The solid curve represents the calculated result using Eq. (12) and the parameters given in the fourth row of Table III.

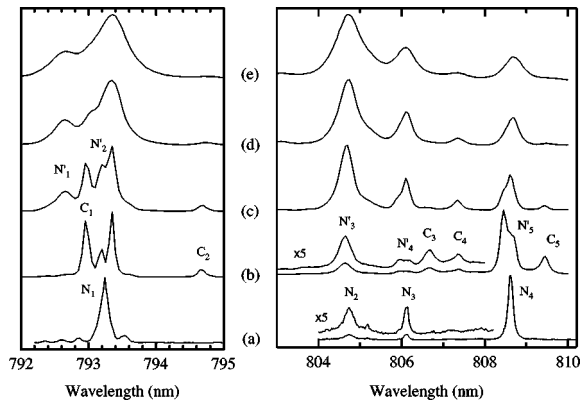

FIG. 9. A portion of the ambient pressure $^3H_4 \rightarrow {}^3H_6$ luminescence of Tm^{3+} in (a) Tm^{3+}(2 at. %):YAG ($\lambda_{ex}=465.8$ nm) and (b)–(e) Cr^{3+}(0.7 at. %):Tm^{3+}(2 at. %):YAG ($\lambda_{ex}=580$ nm) at several temperatures: (a) and (b) $T=15$ K; (c) $T=75$ K; (d) $T=130$ K; (e) $T=175$ K. N_1 (793.24 nm): $W_1 \rightarrow Z_1$, N_2 (804.74 nm): $W_2 \rightarrow Z_3$, N_3 (806.12 nm): $W_2 \rightarrow Z_4$, N_4 (808.62 nm): $W_1 \rightarrow Z_4$; N_1' (792.65 nm): $W_2 \rightarrow Z_2$, N_2' (793.20 nm, 793.35 nm): $W_1 \rightarrow Z_1$, N_3' (805.95 nm): $W_2 \rightarrow Z_3$, N_4' (805.95 nm, 806.15 nm): $W_2 \rightarrow Z_4$, N_5' (808.45 nm, 808.65 nm): $W_1 \rightarrow Z_4$; C_1 (792.95 nm): $W_1 \rightarrow Z_1$, C_2 (794.65 nm): $W_1 \rightarrow Z_2$, C_3 (806.65 nm): $W_1 \rightarrow Z_3$, C_4 (807.35 nm): $W_2 \rightarrow Z_4$, C_5 (809.45 nm): $W_1 \rightarrow Z_4$.

We continued by quantitatively analyzing the experimental-transfer rate data (Fig. 8) as a function of pressure using the model represented by Eq. (12). We specifically incorporated the pressure dependence of the $^4T_2$-^2E energy separation, $\Delta=\Delta_0+(d\Delta/dP)P$, where Δ_0 is the ambient pressure $^4T_2$-^2E energy separation and the shift rate $d\Delta/dP=10$ cm^{-1}/kbar was obtained from previous work.[17,31] A simple calculation was made using Eq. (12) and the values for W_{DA}^{E}, W_{DA}^{T}, $W_{DA}^{AS}(\infty)$, and Δ_0 obtained from the temperature study (Table III, 4th row). The parameter values were taken directly from the temperature study and were not varied when analyzing the pressure results. A comparison between the calculated result and the experimental data is shown in Fig. 8. Excellent agreement with the data was obtained.

D. Acceptor emission and decay at ambient pressure

In an energy-transfer process between donor and acceptor ions, the luminescence and decay properties of the acceptor ions can provide complementary information about the energy-transfer mechanism. We completed additional luminescence and decay experiments on Tm^{3+}:YAG and Cr^{3+}:Tm^{3+}:YAG at low temperature in an attempt to gain further insight into the $Cr^{3+} \rightarrow Tm^{3+}$ energy-transfer mechanism.

A direct comparison of Tm^{3+} luminescence ($^3H_4 \rightarrow {}^3H_6$) obtained by direct excitation ($^3H_6 \rightarrow {}^1G_4$) of Tm^{3+}:YAG and by energy transfer from Cr^{3+} in Cr^{3+}:Tm^{3+}:YAG is shown in Fig. 9. Figures 9(a) and (b) show the Tm^{3+} emission at 15 K in Tm^{3+}:YAG and Cr^{3+}:Tm^{3+}:YAG, respectively. The spectrum of Tm^{3+}:YAG consisted of four principal transitions ($N_1 - N_4$). The transitions can be readily assigned to the $W_1 \rightarrow Z_1(N_1)$, $W_2 \rightarrow Z_3(N_2)$, $W_2 \rightarrow Z_4(N_3)$, and $W_1 \rightarrow Z_4(N_4)$ transitions (where Z_i and W_i denote the crystal-field levels of the $^3H_6$ ground state and of the $^3H_4$ excited state, respectively) discussed in Refs. 16, 39 and 49. The N_i lines originate from unperturbed Tm^{3+} ions at the normal dodecahedral Y^{3+} (c) sites (N-type centers with D_2 site symmetry) in Tm^{3+}:YAG.[16,39–41]

In Cr^{3+}:Tm^{3+}:YAG, Tm^{3+} exhibited a more complicated luminescence spectrum consisting of two groups of luminescence lines labeled C_i and N_i' (Fig. 9). The C_i and N_i' luminescence lines have been attributed to normal Tm^{3+} (c) sites that are perturbed by the presence of Cr^{3+} (a) ions in the first, second, and/or third coordination shells.[10,15,16,20] According to the electric dipole selection rules in regular D_2 symmetry, transitions between crystal field levels described by identical irreducible representations are forbidden ($\Gamma_{\alpha,J'} \not\leftrightarrow \Gamma_{\alpha,J''}$). The presence of the C_2 ($W_1 \rightarrow Z_2$) line, representing a transition between two states with Γ_1 symmetry, indicates that the site symmetry of the C-type Tm^{3+} centers deviates from the regular D_2 site symmetry due to the perturbation of nearby Cr^{3+} ions. Lupei and co-workers[16,20] suggested that the C-type centers result from ion pairs between a Tm^{3+} (c) ion and a Cr^{3+} (a) ion in the first coordination shell (with a distance of 3.354 Å in YAG). Figure 9 further indicates the presence of N_i' lines. Each labeled N' lines consists of two components indicating the likely presence of two distinct N'-type centers. Since the energies of the N_i lines are very close to the energies of corresponding N_i lines in Fig. 9(a), we expect that N'-type centers in Cr^{3+}:Tm^{3+}:YAG are very similar to the regular N-type Tm^{3+} centers found in Tm^{3+}:YAG and likely result from a weak local perturbation caused by distant Cr^{3+} ions in the second or the third coordination shells around Tm^{3+}. In the following discussion, we make no attempt to distinguish different N'-type centers.

Figure 9 also shows the temperature dependence of the Tm^{3+} luminescence in Cr^{3+}:Tm^{3+}:YAG excited through $Cr^{3+} \rightarrow Tm^{3+}$ energy transfer. We observed (i) that at low

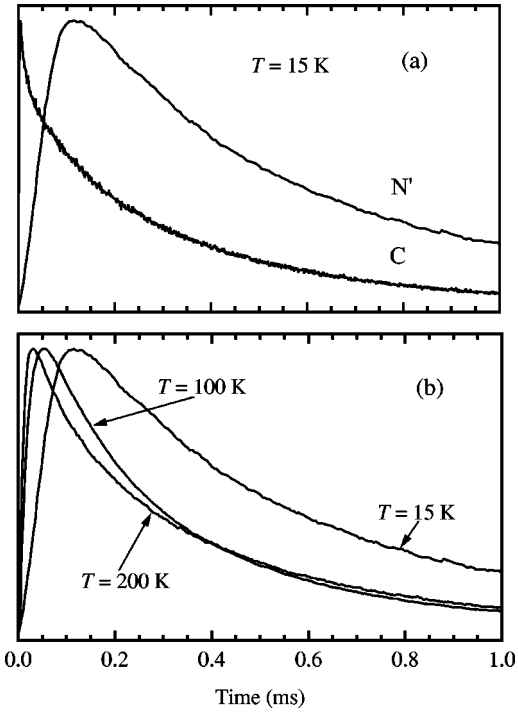

FIG. 10. Ambient pressure luminescence decays of Tm^{3+} in Cr^{3+}(0.7 at. %):Tm^{3+}(2 at. %):YAG following energy transfer upon excitation of Cr^{3+} ($^4A_2 \rightarrow {}^4T_2$) ($\lambda_{ex}=580.0$ nm). (a) Luminescence decays of *C*- and *N'*-type Tm^{3+} centers at 15 K and (b) luminescence decays of *N'*-type Tm^{3+} centers at 15, 100, and 200 K.

temperature, the luminescence intensity is comparable for the *C*-type and *N'*-type Tm^{3+} centers; (ii) that with increasing temperature, the luminescence of the *N'*-type centers increases much more strongly than that of *C*-type centers; and (iii) that the *N'*-type centers dominate the Tm^{3+} luminescence above ~100 K. The experimental results for the temperature dependence of the Tm^{3+} luminescence reveal that the number of energy-transfer events from Cr^{3+} to *C*- and *N'*-type Tm^{3+} centers is comparable at lower temperatures and that the number of energy-transfer events from Cr^{3+} to *N'*-type centers relative to *C*-type centers increases significantly with increasing temperature. The results indicate that the room-temperature $Cr^{3+} \rightarrow Tm^{3+}$ energy-transfer process in Cr^{3+}:Tm^{3+}:YAG is controlled by the *N'*-type Tm^{3+} acceptor centers.

The $^3H_4 \rightarrow {}^3H_6$ luminescence decays of the *C*- and *N'*-type Tm^{3+} centers at 15 K showed distinctly different time dependences [Fig. 10(a)]. The luminescence from the *C*-type centers starts almost immediately after pumping the Cr^{3+} donor ions, while the luminescence from the *N'*-type centers exhibited an obvious rise before decaying. This fact indicates that the energy transfer from Cr^{3+} donor ions to *C*-type acceptor centers is much faster than to *N'*-type acceptor centers and supports the assignment of *C*- and *N'*-type centers to Tm^{3+} acceptor sites that are in close and more distant proximity, respectively, to perturbing Cr^{3+} ions. We also observed a strong effect of temperature on the *N'*-type center luminescence [Fig. 10(b)]. Within the approximation of the transfer function $P_{DA}(t)$ as a linear function of time (Sec. III A) and using Eqs. (8) and (9) for the *N'*-type Tm^{3+} centers, we obtained $W_A \approx 2.2\times10^3\ s^{-1}$, $\bar{W}_{DA} \approx 2.7\times10^4\ s^{-1}$, $t_{max} \approx 122\ \mu s$ at 15 K; $W_A \approx 3.9\times10^3\ s^{-1}$, $\bar{W}_{DA} \approx 6.6\times10^4\ s^{-1}$, $t_{max} \approx 51\ \mu s$ at 100 K; and $W_A \approx 3.8\times10^3\ s^{-1}$, $\bar{W}_{DA} \approx 2.2\times10^5\ s^{-1}$, $t_{max} \approx 26\ \mu s$ at 200 K.

E. Inokuti-Hirayama approximation

Inokuti and Hirayama[35] used a continuum approximation in the context of the multipolar energy-transfer mechanism to obtain the energy-transfer function as

$$P_{DA}(t) = \frac{4}{3}\pi\Gamma\left(1-\frac{3}{m}\right)c_A[\alpha_{DA}^{(m)}t]^{3/m}, \tag{13}$$

where $\Gamma(x)$ is Euler's gamma function and c_A is the concentration (number density) of acceptors. The $t^{3/m}$ dependence of the transfer function is commonly used to describe donor decays in energy-transfer processes. In principle, the multipolar exponent *m* of the transfer mechanism can be determined from Eq. (13), if very accurate decay measurements are available.[2,3]

The validity of Eq. (13), however, requires a uniform (statistically random) distribution of acceptors in the lattice. A random distribution of acceptors around donors will occur if no donor-acceptor interactions exist. Noninteracting donors and acceptors imply that the presence of a donor ion in a given lattice site has no influence on the likelihood of acceptor ions locating nearby during crystal growth. When donors and acceptors interact, it becomes possible for the donor to influence the location of acceptors. An attractive interaction increases the likelihood that an acceptor will preferentially occupy sites adjacent to the donor (correlated placement), while a repulsive interaction increases the likelihood that an acceptor will preferentially occupy sites far removed from the donor (uncorrelated placement).[50] Equation (4), rather than Eq. (13), should be used to analyze energy transfer when the distribution of acceptors is unknown.[3,45]

In the previous temperature (78–350 K) (Ref. 8) and pressure (ambient–80 kbar)[17] studies of energy transfer in Cr^{3+}:Tm^{3+}:YAG, it was observed that the Inokuti-Hirayama dipole-dipole treatment became increasingly unsatisfactory at either low temperature or high pressure. As discussed in the preceding section, multiple Tm^{3+} sites are present in Cr^{3+}:Tm^{3+}:YAG. In *C*-type sites, Tm^{3+} ions are spatially close to Cr^{3+} ions and in *N'*-type sites, they are further removed and more closely resemble a random distribution. The measurable presence of *C*-type sites indicates a nonrandom placement of acceptors in Cr^{3+}:Tm^{3+}:YAG. We therefore expect a breakdown of the Inokuti-Hirayama model under conditions in which local energy transfer to *C*-type sites is comparable to or dominates distant energy transfer to *N'*-type sites.

The determination of the relative importance of energy transfer to *C*-type and *N'*-type sites requires a consideration of the rate of transfer from Cr^{3+} to *C*-type sites relative to *N'*-type sites and the relative concentrations of the two types of acceptor sites in the lattice. Since energy-transfer rates increase with decreasing donor-acceptor distance (cf. Table I), we know that the transfer rate to *C*-type sites will be faster (Fig. 10 clearly supports this point). The concentration of

C-type sites, however, will be lower because the total number of possible acceptor sites in close proximity to a donor is small. It is therefore possible for N'-type sites to dominate energy transfer on the basis of their much higher concentration even though their energy-transfer rate is slower than that of *C*-type sites. We consequently expect the Inokuti-Hirayama model to breakdown when local energy transfer to *C*-type sites accounts for a significant portion of the total energy transfer and to become increasingly valid as distant energy transfer to N'-type sites becomes more important.

The occurrence of distant energy transfer depends on its rate relative to the intrinsic donor decay rate (W_D). Regardless of the local energy-transfer rate, distant energy transfer will occur when local acceptors become saturated as long as the distant energy-transfer process competes favorably with the intrinsic decay process of the donor. Our experiments indicate that external conditions influence the relative importance of local and distant energy-transfer processes. The low-temperature breakdown of the Inokuti-Hirayama model[8] indicates that local-energy transfer is significant at low temperature [Fig. 9(b) supports this conclusion]. The significant contribution of *C*-type sites to the energy-transfer process suggests that energy transfer to N'-type sites does not compete favorably with intrinsic Cr^{3+} decay at low temperature. This is the likely origin of the relative low overall energy-transfer rate at low temperatures (Fig. 5). When we increase the temperature, we produce strong anti-Stokes and $^4T_2$ emission intensity that efficiently overlaps the $^3F_{2,3}$ states of Tm^{3+} and greatly increases the energy-transfer rate (Fig. 5). Figure 9 indicates that the additional energy transfer is to the distant N'-type sites. Presumably, transfer to the *C*-type sites saturates and further transfer necessarily occurs to the more distant N'-type sites. The improved spectral overlap at higher temperatures (Figs. 3 and 6) suggests a significantly increased rate of distant energy transfer relative to internal Cr^{3+} decay despite the factor of ~6 increase in the internal Cr^{3+} decay rate between 15 K and RT resulting from the increased population of the $^4T_2$ state (Table II). As a result, the Inokuti-Hirayama treatment becomes a more reasonable model as the temperature approaches room temperature.

Similar reasoning holds for the pressure experiment. An increase of pressure at room temperature leads to an increase in the energy of the $^4T_2$ state relative to the ^2E state, a reduction of $^4T_2$ thermal population, and a consequent decrease of $^4T_2$ emission intensity. Since the lost $^4T_2$ intensity efficiently overlaps the $^3F_{2,3}$ absorption bands of Tm^{3+}, energy transfer becomes less effective at high pressure and a decrease in overall transfer rate results (Fig. 8). A lower energy transfer rate at high pressure suggests that the less effective energy transfer process to the distant N'-type centers is diminished and that a larger fraction of energy-transfer events occurs locally to the nonrandom *C*-type centers. As a result, the Inokuti-Hirayama treatment becomes increasingly less applicable with pressure.

F. Resolution of competing energy-transfer pathways

The constancy of the energy-transfer properties from the ^2E state with pressure allows us to resolve the different contributions to energy transfer in Cr^{3+}:Tm^{3+}:YAG at ambient conditions based on comparisons with limiting low-temperature and high-pressure behavior. At ambient conditions, energy transfer can occur from the ^2E zero phonon and Stokes sideband transitions, the ^2E anti-Stokes sideband transitions, and the $^4T_2$ state. Our experiments indicate that these three contributions are influenced differently by pressure and temperature. The ^2E zero-phonon line and Stokes sideband emission energy and intensity are approximately independent of temperature and pressure. The ^2E anti-Stokes sideband intensity depends on temperature, but is approximately independent of pressure. The $^4T_2$ intensity depends on both temperature and pressure.

By increasing pressure at room temperature, we can therefore eliminate the $^4T_2$ energy-transfer contribution without affecting any component of the ^2E energy-transfer contribution. The difference in ambient pressure transfer rate ($\sim 400\ ms^{-1}$) and the limiting high-pressure transfer rate ($\sim 95\ ms^{-1}$) at room temperature (Fig. 8) provides a quantitative measure of the importance of the $^4T_2$ state to energy transfer at ambient conditions. Low temperatures eliminate both the $^4T_2$ and ^2E anti-Stokes contributions to energy transfer. As a result, the difference between the limiting high-pressure transfer rate at RT ($\sim 95\ ms^{-1}$, Table IV and Fig. 8) and limiting low-temperature transfer rate at ambient pressure ($\sim 10\ ms^{-1}$, Table II and Fig. 5) gives an indication of the ^2E anti-Stokes contribution to energy transfer at ambient conditions. The limiting low-temperature rate itself is a measure of energy transfer due to the ^2E zero-phonon and Stokes sideband transitions. We therefore see that most of the energy transfer at ambient conditions is due to the $^4T_2$ state even though it is $\sim 800\ cm^{-1}$ higher in energy than the ^2E state.

IV. CONCLUSIONS

Variable temperature and pressure studies of energy transfer in Cr^{3+}:Tm^{3+}:YAG have been used to probe and resolve underlying contributions to energy transfer. The temperature studies indicate three regimes of behavior: A low-temperature regime (below ~70 K) in which energy transfer from the zero-phonon and Stokes sideband transitions of the ^2E state of Cr^{3+} dominate; an intermediate temperature regime (~70–~175 K) in which the important contribution of thermally activated anti-Stokes ^2E intensity has been revealed; and a high-temperature regime (above ~175 K) in which energy transfer from a thermally populated $^4T_2$ state dominates. Energy-transfer rates in each of the three regimes were quantitatively modeled using Förster-Dexter theory. Between ambient pressure and ~60 kbar, high pressure led to a reduction and an eventual elimination of the contribution of the $^4T_2$ state to the energy-transfer process as the energy of the $^4T_2$ state was increased relative to the ^2E state. Consequently, a decrease in the overall energy-transfer rate from Cr^{3+} between ambient pressure and ~60 kbar was observed. Above ~60 kbar, energy transfer occurred exclusively from the ^2E state and the energy-transfer rate remained approximately constant upon a further increase in pressure. A comparison of the limiting high pressure, limiting low temperature, and ambient condition transfer rates allowed us to separate and determine the relative importance of energy transfer from the ^2E zero-phonon and sideband transitions,

^2E anti-Stokes sideband transition, and $^4T_2$ state at ambient conditions. We found that the importance of the three energy-transfer pathways decreased in the following order at ambient conditions: $^4T_2$ transfer ($\sim$76% of transfer events) $>^2E$ anti-Stokes sideband transfer ($\sim$21%) $>^2E$ zero phonon and Stokes sideband transfer ($\sim$3%).

Our studies also showed that the presence of closely associated Cr^{3+}-Tm^{3+} pairs was responsible for a breakdown of the Inokuti-Hirayama model of energy transfer at low temperature or high-pressure conditions. At low temperature or high pressure, a low overall energy-transfer rate increased the importance of energy transfer from Cr^{3+} to the closely associated Tm^{3+} ions relative to randomly distributed, more distant Tm^{3+} sites. Under these conditions, the Inokuti-Hirayama model failed. At high temperature or low pressure, however, the energy-transfer rate was sufficiently enhanced to permit efficient transfer to the more numerous randomly distributed Tm^{3+} sites and the Inokuti-Hirayama model adequately described the energy-transfer data.

ACKNOWLEDGMENTS

We gratefully acknowledge primary financial support from the National Science Foundation under Grant No. DMR-9629990. Partial financial support was also provided by the U. S. Department of Energy under Grant No. DE-FG03-97SF21388. We wish to express our thanks to P. Wamsley for her initial high-pressure luminescence measurements.

[1] R.T. Wegh, H. Donker, K.D. Oskam, and A. Meijerink, Science **283**, 664 (1999).
[2] B. Di Bartolo, *Energy Transfer Processes in Condensed Matter*, Vol. 114 of *NATO Advanced Study Institute, Series B: Physics*, edited by B. Di Bartolo (Plenum Press, New York, 1984), p. 103.
[3] A. Henderson and G. Imbusch, *Optical Spectroscopy of Inorganic Solids* (Clarendon Press, Oxford, 1989).
[4] T. Föster, Ann. Phys. (Leipzig) **2**, 55 (1948).
[5] D.L. Dexter, J. Chem. Phys. **21**, 836 (1953).
[6] V.A. Smirnov and L.A. Shcherbakov, IEEE J. Quantum Electron. **24**, 949 (1988).
[7] P.F. Moulton, J.G. Manni, and G.A. Rines, IEEE J. Quantum Electron. **24**, 960 (1988).
[8] G. Armagan, B. Di Bartolo, and A.M. Buoncristiani, J. Lumin. **44**, 129 (1989); **44**, 141 (1989).
[9] R. Reisfeld, *Spectroscopy of Solid-State Laser-Type Materials*, edited by B. Di Bartolo, International Science Series Vol. 30 (Plenum Press, New York, 1992), p. 343.
[10] W. Nie, Y. Kalisky, C. Pédrini, A. Monteil, and G. Boulon, Opt. Quantum Electron. **22**, S123 (1990); W. Nie, A. Monteil, and G. Boulon, *ibid.* **22**, S227 (1990).
[11] J.A. Mares, W. Nie, and G. Boulon, J. Lumin. **48/49**, 227 (1991).
[12] A. Brenier, C. Madej, C. Pédrini, and G. Boulon, *Optical Properties of Excited States in Solids*, Vol. 301 of *NATO Advanced Study Institute, Series B: Physics*, edited by B. Di Bartolo (Plenum Press, New York, 1992), p. 445.
[13] A. Brenier, G. Boulon, C. Pédrini, and C. Madej, Opt. Mater. **1**, 299 (1992).
[14] I. Vergara, E. Camarillo, J.A. Sanz-García, J. García Solé, F. Jaque, A. Monteil, and G. Boulon, Solid State Commun. **82**, 733 (1992).
[15] V. Lupei, L. Lou, G. Boulon, A. Lupei, and C. Tiseanu, J. Phys. I **3**, 1245 (1993).
[16] A. Lupei, C. Tiseanu, and V. Lupei, Phys. Rev. B **47**, 14 084 (1993).
[17] P.R. Wamsley and K.L. Bray, in *New Materials for Advanced Solid-State Lasers*, edited by B.H.T. Chai, S.A. Payne, T.Y. Fan, A. Cassanho, and T.H. Allik, MRS Symposia Proceedings No. 329 (Materials Research Society, Pittsburgh, 1994), p. 85; P.R. Wamsley and K.L. Bray, J. Lumin. **63**, 31 (1995).
[18] A. Brenier, C. Madej, C. Pédrini, and G. Boulon, Chem. Phys. Lett. **233**, 451 (1995).
[19] P. Hong, X.X. Zhang, C.W. Struck, and B. Di Bartolo, J. Appl. Phys. **78**, 4659 (1995).
[20] V. Lupei, A. Lupei, and G. Boulon, Phys. Rev. B **53**, 14 818 (1996).
[21] E. Luria, S.R. Rotman, J.A. Mares, G. Boulon, A. Brenier, and L. Lou, J. Lumin. **72-74**, 951 (1997).
[22] G. Huber, E.W. Duczynski, and K. Petermann, IEEE J. Quantum Electron. **24**, 920 (1988).
[23] E.W. Duczynski, G. Huber, V.G. Ostroumov, and I.A. Shcherbakov, Appl. Phys. Lett. **48**, 1562 (1986).
[24] G. Huber, E.W. Duczynski, P. Mitzscherlich, and H.O. Teichmann, J. Phys. Colloq. **48**, C7-309 (1987).
[25] B. Struve and G. Huber, Appl. Phys. B: Photophys. Laser Chem. **36**, 195 (1985).
[26] B. Henderson, A. Marshall, M. Yamaga, K.P. O'Donnell, and B. Cockayne, J. Phys. C **21**, 6187 (1988).
[27] S.J. Duclos, Y.K. Vohra, and A.L. Ruoff, Phys. Rev. B **41**, 5372 (1990).
[28] A.G. Rinzler, J.F. Dolan, L.A. Kappers, D.S. Hamilton, and R.H. Bartram, J. Phys. Chem. Solids **54**, 89 (1993).
[29] P.T.C. Freire, O. Pilla, and V. Lemos, Phys. Rev. B **49**, 9232 (1994).
[30] D. de Viry, J.P. Denis, N. Tercier, and B. Blanzat, Solid State Commun. **63**, 1183 (1987).
[31] P.R. Wamsley and K.L. Bray, J. Lumin. **59**, 11 (1994).
[32] U. Hömmerich and K.L. Bray, Phys. Rev. B **51**, 12 133 (1995).
[33] J.H. Eggert, K.A. Goettel, and I.F. Silvera, Phys. Rev. B **40**, 5724 (1989); **40**, 5733 (1989).
[34] Y.R. Shen and K.L. Bray, Phys. Rev. B **56**, 10 882 (1997).
[35] M. Inokuti and F. Hirayama, J. Chem. Phys. **43**, 1978 (1965).
[36] W.A. Wall, J.T. Karpick, and B. Di Bartolo, J. Phys. C **4**, 3258 (1971).
[37] I.N. Douglas, Phys. Status Solidi A **9**, 635 (1972).
[38] J.P. Hehir, M.O. Henry, J.P. Larkin, and G.F. Imbusch, J. Phys. C **53**, 2241 (1974).
[39] J.B. Gruber, M.E. Hills, R.M. Macfarlane, C.A. Morrison, G.A. Turner, G.J. Quarles, G.J. Kintz, and L.A. Esterowitz, Phys. Rev. B **40**, 9464 (1989).
[40] C. Tiseanu, A. Lupei, and V. Lupei, J. Phys.: Condens. Matter **7**, 8477 (1995).

[41] S. Guy, M. Malinowski, Z. Frukacz, M.F. Joubert, and B. Jacquier, J. Lumin. **68**, 115 (1996).
[42] P.R. Wamsley and K.L. Bray, J. Lumin. **60/61**, 188 (1994).
[43] G. Armagan, A.M. Buoncristiani, and B. Di Bartolo, Opt. Mater. **1**, 11 (1992).
[44] D.L. Huber, Phys. Rev. B **20**, 2307 (1979).
[45] J. Klafter, *Energy Transfer Processes in Condensed Matter* (Ref. 2), p. 621.
[46] S.M. Healy, C.J. Donnelly, G.F. Imbusch, and G.P. Morgan, J. Lumin. **46**, 1 (1990).
[47] H. Hua, S. Mirov, and Y.K. Vohra, Phys. Rev. B **54**, 6200 (1996).
[48] F. Euler and J.A. Bruce, Acta Crystallogr. **19**, 971 (1965).
[49] G.H. Dieke, *Spectra and Energy Levels of Rare Earth Ions in Crystals* (Wiley, New York, 1968).
[50] S.R. Rotman, Y. Kalisky, A. Brenier, C. Pedrini, G. Boulon, and F.X. Hartmann, J. Appl. Phys. **72**, 224 (1992).